Model-Based Process Planning for Laser Cutting Operations Under Unsteady-State Conditions

Paul Di Pietro
School of Mechanical and Manufacturing Engineering, University of New South Wales
Sydney, NSW, Australia

Y. Lawrence Yao
Department of Mechanical Engineering, Columbia University
New York, NY 10027

ABSTRACT

Boundary encroachment or cutting right up to pre-cut sections are examples of unsteady-state operations of the laser cutting process. Cornering and generating small diameter holes also fall into this category. Heat transfer is often frustrated here, resulting in bulk heating of the workpiece. This in turn leads to a degradation of the cut quality. Currently, trial-and-error based experimentation is needed in order to assure quality in these regions. Thus model-based process planning has the benefit of reducing this step whilst leading to an optimal solution. Numerical investigation of the laser-workpiece interaction zone quantifies significant effects of such transiency on cutting front mobility and beam coupling behavior. Non-linear power adaptation profiles are generated via the optimization strategy in order to stabilize cutting front temperatures. Experimental results demonstrate such process planning can produce quality improvements.

INTRODUCTION

Laser cutting of complex and intricate workpieces has been common. Of concern though, is the effect of cut geometry on the quality achievable. Boundary encroachment, cornering and contouring often result in severe heat accumulation. This can result in poor quality in the form of widespread burning, increased surface roughness and heat affected zone, and kerf widening.

A review of the efforts towards better understanding and quality improvement in the laser cutting process was given (Di Pietro and Yao, 1994). In particular, Gonsalves and Duley (1972) first accounted for the fact that only part of the incident beam power is available for laser cutting sheet metals. Powell (1993) devised cutting experiments to investigate the transmission and reflection losses occurring in the cutting process based on previous work done by Miyamoto, Maruo and Arata (1984, 1986). Schreiner-Mohr, et al. (1991) also conducted experimental work which showed that at maximum cutting speeds, the beam center can precede the front location. At slow cutting speeds the beam center was shown to lag behind the cutting front. A mono-dimensional finite difference model was proposed by Yuan, Querry, and Bedrin (1988) which suggested that the cutting front could possess mobility when cutting at constant processing speeds. Arata et al. (1979) showed through high speed photography that the cutting front was indeed dynamic in nature. Laser cutting of curved trajectories has been studied by Sheng and Cai, 1994. It was shown that circular laser cutting produces larger kerf width, shifted centerline towards the center of rotation, and larger inner kerf wall taper.

Systems which allow the adaptation of laser power when cornering to compensate for the reduced cutting speeds associated there have been available (e.g., Steen and Li, 1988, and Powell, 1993). One method of achieving this control feature is by varying the pulse frequency and/or duty cycle proportionally to the feedrate (e.g., Moriyasu et al., 1986, Schuocker and Steen, 1986). The determination of this power-feed ratio currently relies on experimentation. In order to obtain sharp edges on curved trajectories, pulsed mode operation is also commonly employed. The problem with this is that heat-affected zones are almost doubled in extent compared to using continuous wave power (Geiger et al., 1988). This is explained by the more gradual temperature gradients experienced when pulsing the laser beam.

In this paper, a transient model is developed to investigate the effects of cut geometry (e.g., boundary encroachment, cornering or cutting small holes) on cutting front dynamic phenomena,

especially cutting front speed, temperature and transmitted power fluctuations. Its effect on heat affected zone extent is also studied. Numerical solutions of the model are compared with experimental results. Finally, a power adaptation strategy is implemented to improve quality in these regions.

MODELING STRATEGY

A detailed description of the mathematical formulation has been presented elsewhere (Di Pietro and Yao, 1995a). A brief summary is given below for completeness. In order to focus on the development of optimization, constant thermo-physical properties and two-dimensional transient heat conduction are simply assumed. Realistic boundary conditions which allow convection and radiation to occur to the surroundings are considered. This results in the following equation:

$$\frac{K}{\rho c_v}\left(\frac{\partial^2 T}{\partial x^2}+\frac{\partial^2 T}{\partial y^2}\right)+\frac{\partial T}{\rho c_v \partial z}(h_f+h_n+2h_r)+\frac{\dot{q}}{\rho c_v}=\frac{\partial T}{\partial t} \qquad (1)$$

where K = thermal conductivity, ρ = density, c_v = heat capacity, forced convective heat transfer coefficient $h_f = Nu_d\, K / d$ and Nusselt number $Nu_d = 0.027\, Re_d^{0.8}\, Pr^{0.33}\, (\mu_m / \mu_w)^{0.14}$(White, 1988). At all points other than where the oxygen gas jet impinges, it is assumed that there is no farfield streaming and thus natural or free convection occurs. However underneath the cutting nozzle, forced convection is apparent and the resultant heat flux will generally be far greater than in the free convection case. Fully developed turbulent flow in a smooth tube is assumed for the forced convection case. h_n is the free convection contribution (relatively small), and h_r the radiative heat transfer coefficient.

The material removal process is in actual fact a rather complex interaction of the gas jet on the free surface of the melt, where shear stresses act on the cutting front and a boundary layer exists. It is assumed in our model that any area in the molten state is expelled out of the kerf immediately, by the force of the gas jet. The CO_2 laser source is assumed to be of Gaussian TEM_{oo} mode. The energy produced by the exothermic reaction is considered. Assuming a pure oxygen supply for the assist gas, the following reaction occurs within the cutting kerf: $Fe + 0.5O_2 = FeO$ (Powell et al., 1992) and ΔH = -257.58 kJ/mol, where ΔH is the energy released during the reaction and the ignition point is 1473.15K (Geiger et al., 1988).

If the mass removal rate of the melt out of the kerf is known or can be calculated, then the following relationship can be used to determine the energy obtained by reaction.

$$P_{exo} = \text{ratio}\left(\frac{\dot{m}\,\Delta H}{\text{amu}}\right) \qquad (2)$$

where amu = 1 mole FeO = 71.847 g/mol and ratio is the percentage of FeO:Fe ejected from the kerf. It has been assumed previously that the material removal rate $\dot{m}$ can be given approximately by the following equation (Schuocker, 1988): $\dot{m} = \rho b D V_b$ where b = kerf width, D = workpiece thickness and V_b = velocity of laser beam. This is only true though when it is assumed that the processing speed equals the front speed as in steady state cutting. In reality though, the mass removal rate is more appropriately given as:

$$\dot{m} = \rho b D V_f \qquad (3)$$

where V_f = cutting front velocity which physically represents the solid-liquid interface speed, as all the molten material is assumed to be ejected out of the bottom of the kerf immediately.

Numerical determination of cutting front velocity:

From Fig. 1(a), it can be shown that:

$$V_f = V_b + \frac{\partial S}{\partial t} \qquad (4)$$

where $\partial S/\partial t$ is the time rate of change of the molten layer thickness. The molten layer thickness is given by the shortest distance from the melting isotherm to the laser beam's center at any given time t. A numerical expression for the average time rate of change of the molten layer thickness over the interval Δt can be obtained for evaluating the front velocity by using a method of first order interpolation between the nodal temperature T_m and the forward-shifted temperature T_{m+1}. At time $t = j$ and $t+\Delta t = j+1$

$$S^j = \Delta y \frac{(T_m{}^j - T_{melt})}{(T_m{}^j - T_{m+1}{}^j)} \text{ and } S^{j+1} = \Delta y \frac{(T_m{}^{j+1} - T_{melt})}{(T_m{}^{j+1} - T_{m+1}{}^{j+1})} \qquad (5)$$

where m denotes the nodal point of interest.

$$\text{therefore, } \frac{\Delta S}{\Delta t} = \frac{(S^{j+1} - S^j)}{\Delta t} \qquad (6)$$

Knowing V_f also enables numerical determination of fluctuations of the transmitted power. The percentage of power incident on the workpiece is given by the proportion the cutting front is ahead of the trailing edge of the laser beam (Fig. 1b). If the front is behind the trailing edge of the laser beam, then all the beam power will fall on the workpiece. This represents the most efficient beam coupling theoretically possible. In reality though, some beam leakage will always occur.

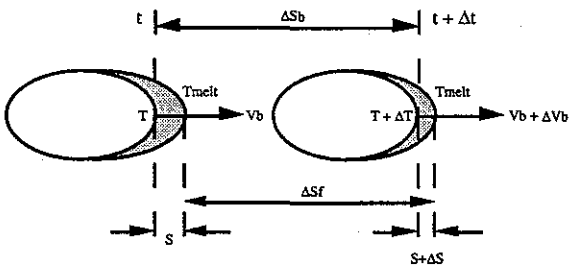

Fig. 1(a) Generation of cutting front mobility.

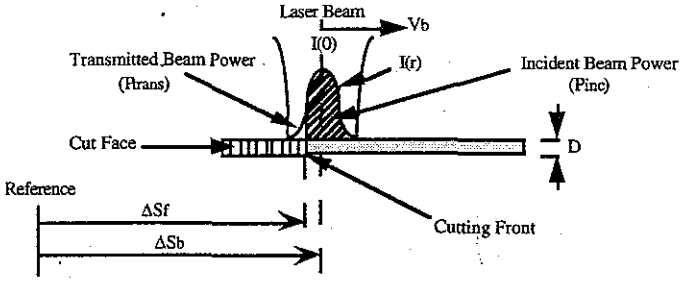

Fig. 1(b) Laser beam transmission losses

AN OPTIMIZATION STRATEGY VIA POWER ADAPTATION

By adapting parameters such as laser power levels, switching between continuous wave and pulsed mode, and effecting cutting speed changes, quality improvements were obtainable. Such techniques are trial-and-error based, whereby the optimal set of parameters may still not be reached.

An optimization strategy is therefore proposed based on the numerical modeling. In the strategy it forces the cutting front temperature to remain steady regardless of the change of cut geometry, e.g., boundary encroachment, cornering or cutting a small hole. The problem of minimizing the deviation from steady state results in a non-linear power profile, as the inter-relationships between laser parameters are complicated by the mobility exhibited by the cutting front.

The strategy developed is iterative by nature. The model proceeds forward in time by the accumulation of the timestep Δt of integration. By monitoring the status of the front temperature at

every instance, a steady state value ΔT can be established, that is, $| T_f^{j+1} - T_f^j | < \Delta T$. The cutting front temperature can be disturbed subsequently by a speed change of the motion system (e.g., cornering) or a change in the workpiece heat accumulation due to cut geometry such as boundary encroachment. As the change in temperature exceeds the previously set limit ΔT, a course of action is required in the form of a power rise or reduction of size $\Delta P_{inc} = k |T_f^{j+1} - T_f^j|$. The size of this power increment is based on two pieces of information forwarded to the optimization module. In order to return the system to its controlled state, the power change to be effected is directly proportional to the temperature deviation observed. This is achieved by the proportionality constant k, which effects the convergence rate of solution. Of course, if the constant is too large, then the temperature cannot be stabilized within the ΔT control limit.

Logically if the cutting front temperature rises, then a power reduction is needed to return the temperature to its previous level. By analogy, a temperature fall requires an increase in power. This conditional test is expressed as follows:

$$\begin{aligned} \text{Condition:} \quad & \{\text{if } (T_f^{j+1} > T_f^j)\}: \quad \Delta P^j = \Delta P^j - \Delta P_{inc} \\ & \{\text{if } (T_f^{j+1} < T_f^j)\}: \quad \Delta P^j = \Delta P^j + \Delta P_{inc} \end{aligned} \qquad (3)$$

From which, an updated cutting front temperature is determined. If it falls within the set allowable temperature tolerance, the model then proceeds forward to the next user-specified beam position whereby the procedure repeats.

SIMULATION AND EXPERIMENTAL CONDITIONS

The following physical quantities and parameters were used in the numerical model: Gaussian TEM_{oo} CO_2, assist gas: O_2, 5" focal lens, K = 51 W/mK, amu = 71.847 g/mol, T_{melt} = 1809.15 K, beam radius R_b = 250 μm, σ_b = 5.67E -8 W/m^2K^4, absorption A_b = 0.4, L_f = 275 kJ/kg, α = 1E -5 m^2/s, ρ = 7865 kg/m^3, ΔH = -257.58 kJ/mol and $\Delta x = \Delta y$ = 125 μm. The following simulation and experimental conditions were used: laser power of 500, 600, and 800 W, and cutting speed of 10, 20, and 30 mm/sec.

The experiments were performed on a fast axial flow 1.5 kW CO_2 laser (PRC FH 1501). The beam mode is essentially TEM_{oo}, with all experiments performed under continuous wave (CW) operation. The laser beam was focused down to 250 μm, through a 5" ZnSe high pressure meniscus lens. The throat diameter of the nozzle used was 1 mm, and a nozzle-standoff distance of 1 mm was maintained. Assist gas pressures were kept constant at 2.7 bar throughout the experiments. Cold rolled mild steel plates (AS 1595) of 1 mm thickness were used.

In order to validate workpiece temperature distributions calculated to those determined experimentally, thermocouples (type K) were used. High speed photography was also undertaken to examine and investigate cutting front mobility on approach to a workpiece boundary. Cine films were taken at a camera speed of 500 frames per second, and a Hitachi camera was focused directly on the laser-material interaction zone. It was positioned perpendicular to the line of cut at an angle of 15^0. Analysis of the developed film was carried out under a Nikon Shadowgraph.

RESULTS AND DISCUSSION

Comparing Workpiece Temperature Distributions

Fig. 2 shows a typical temperature contour plots of the cutting process during boundary encroachment. The isotherms change both in shape and size as time progresses because the model considers multidimensional unsteady heat conduction. Note the presence of the kerf along the center of the workpiece makes the isotherms deviate from the classical 'egg' shaped isotherms that are well known for moving sources of heat. Fig. 3 shows typical progressive temperature contours determined from the numerical model when cornering. Because of the higher

temperatures experienced in the vicinity of the corner point when generating male corners, they are much more susceptible to tip melt-off when compared to their female counterparts.

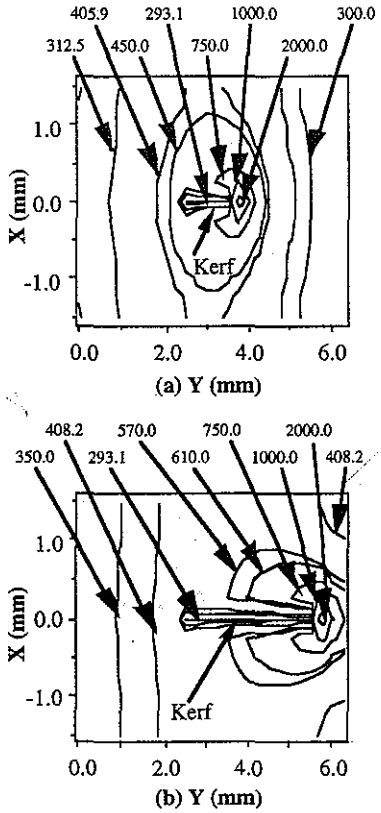

Fig. 2 Simulated temperature distribution during boundary encroachment. (a) 0.144 s (b) 0.178 s (power: 600 W, speed: 20 mm/s)

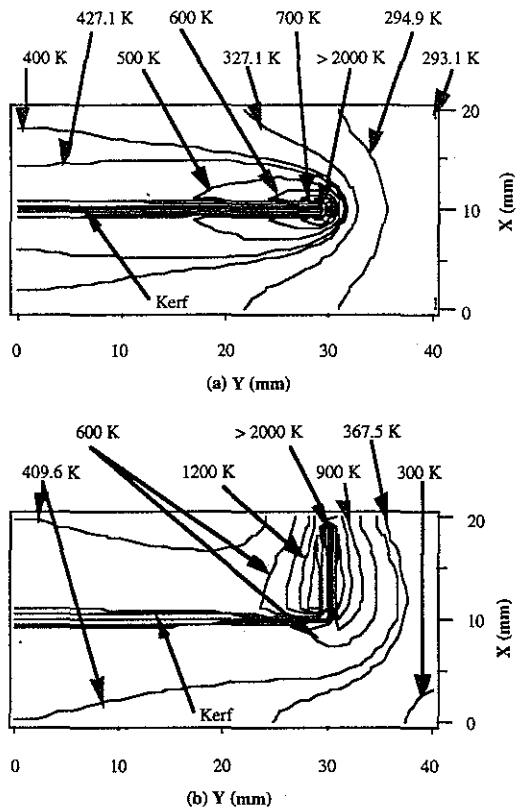

Fig. 3 Simulated temperature distribution during cornering. a) 3.075 s, and b) 4.125 s (power: 800 W, speed: 10 mm/s)

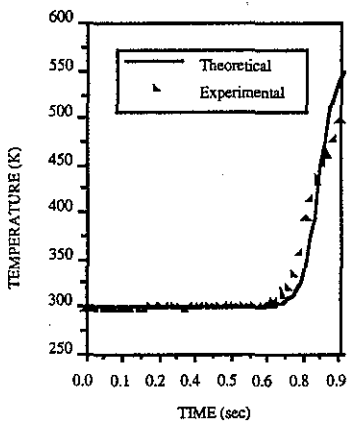

Fig. 4(a) Typical thermocouple measurement as compared to the numerical solution (power: 600 W, speed: 20 mm/s)

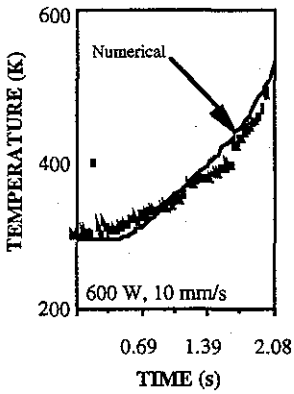

Fig. 4(b) Typical hole cutting temperature measurements (obtained by thermocouples) as compared to simulation results

In order to validate workpiece temperature distributions calculated to those determined experimentally, thermocouples (type K) were used. When approaching a boundary, they were imbedded 1.5 mm in from the boundary edge. Whilst cutting the 5 mm diameter hole, the thermocouples were imbedded 1.5 mm in from the actual workpiece corner point. These were chosen to avoid high temperature gradients closer to the line of cut. Fig. 4(a) shows typical

transience experienced in practice on approach to a prescribed boundary as compared to numerical results while Fig. 4(b) shows temperature rises in the laser hole cutting case.

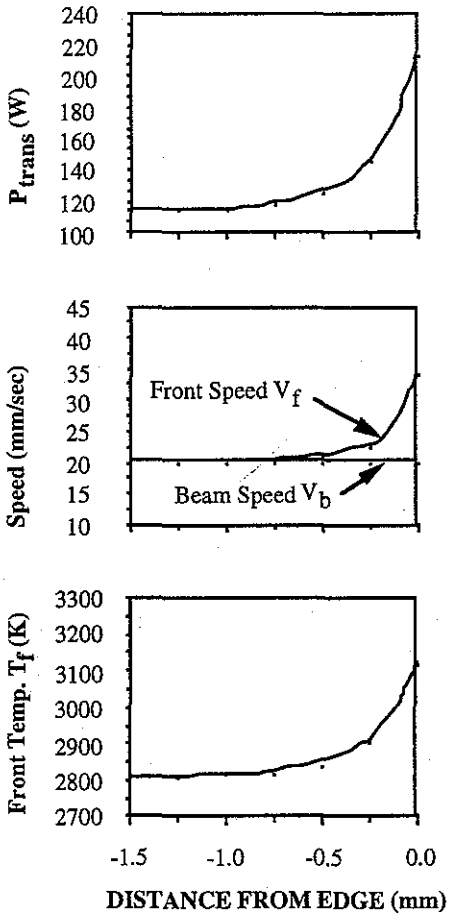

Fig. 5(a) Simulated effect of boundary encroachment
(power: 600 W, speed: 20 mm/s)

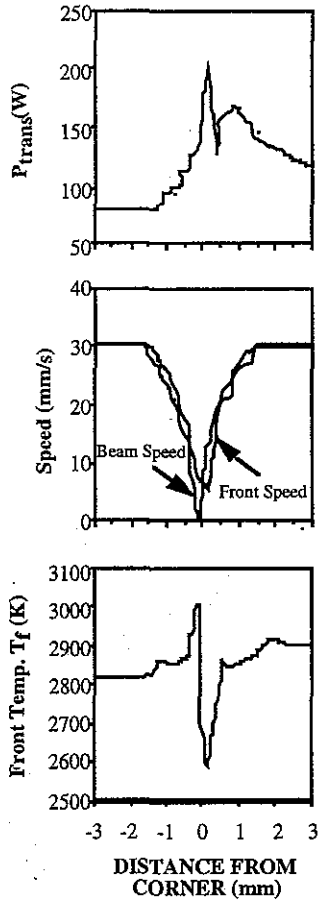

Fig. 5(b) Simulated effect of cornering
(power: 600 W, speed: 30 mm/s)

Transient Effects

Fig. 5(a) shows a typical simulation result for boundary encroachment. Although the cutting speed remains constant right up to the workpiece edge, the front velocity begins to move on its approach to the boundary because heat diffusion is frustrated and over-heating of the area occurs. The increase in the front speed produces an increase in the exothermic power, but this increase in contrast, also results in more power falling through the kerf. The net effect of all these mechanisms working at once is best depicted by the increase in the cutting front temperature experienced by the boundary encroachment (experimentally verified as seen in Fig. 4a).

Fig. 5(b) shows typical simulation results when a corner is part-programmed. It is clear that the transmitted power increases to the corners because of the deceleration of one axis to zero. After the corners, greater beam coupling results because of the acceleration of the other axis to reach the target speed of 30 mm/s. Also note the dynamics of the cutting front, where there is an apparent speed lag behind the processing velocity. The net affect of these two contributions are shown by the complex temperature profiles generated. The contour change involved in processing such routines (viz., the positional relationship of existing boundaries to the kerf's altered directional path), impacts on the transmitted power, front velocity and temperature in that they do not stabilize to their pre-corner, steady-state values but to other levels.

High speed photography was undertaken in order to examine the cutting front mobility on approach to a boundary. By measuring the relative distance moved by the front between frames and knowing the camera speed, an approximate measure of the cut speed could be determined (Fig. 6), and the values were comparable to those determined theoretically.

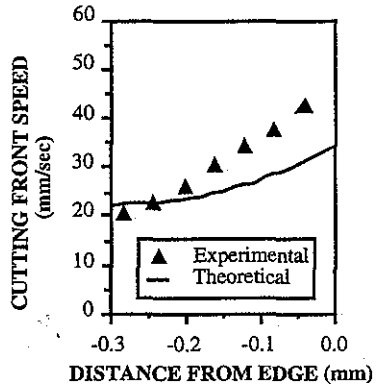

Fig. 6 High speed filming measurement of front mobility on boundary encroachment (power: 600 W, speed: 20 mm/s)

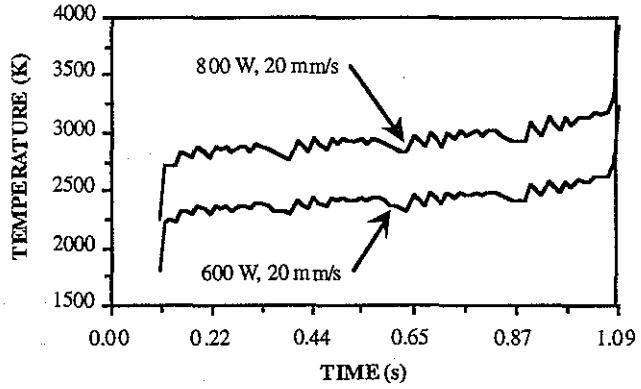

Fig. 7 Simulated cutting front temperatures when a 5 mm circle is represented by using a segmented circle approximation

Fig. 7 shows typical simulation results when the 5 mm hole is approximated. The unusual peaks and valleys are not a random feature of the temperature profiles but reflect the manner in which the motion paths are generated. If curvilinear coordinates were defined, then these irregularities would not appear. Although the processing speed remains constant, the cutting front temperature on average rises gradually as the cut proceeds. In the final stages of the cut, it is clear that the temperature rises markedly due to the frustrated heat accumulation. This is experimentally validated as seen in Fig. 4(b).

POWER MANIPULATION FOR QUALITY IMPROVEMENTS

Fig. 8(a) shows the power levels measured by a probe and its associated discharge current. Current control is via a 12 bit digital word which allows accurate manipulation through part programs generated. Fig. 8(b) shows the response of a resonator discharge to a step input. The output approximates a step response of a first-order system, and the time constant of the system was found as about 1.3 ms. Thus the laser control facility was adequate to perform the optimization power strategies to be implemented under the said experimental conditions.

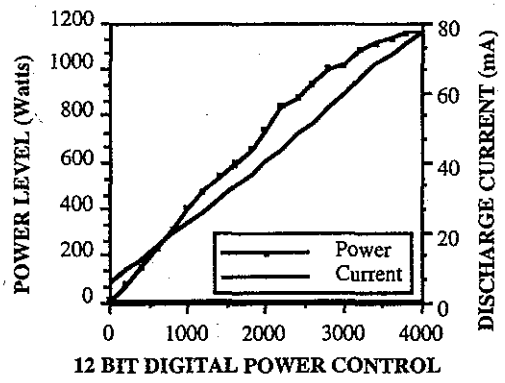

Fig. 8(a) Power levels and discharge current vs. digital control word

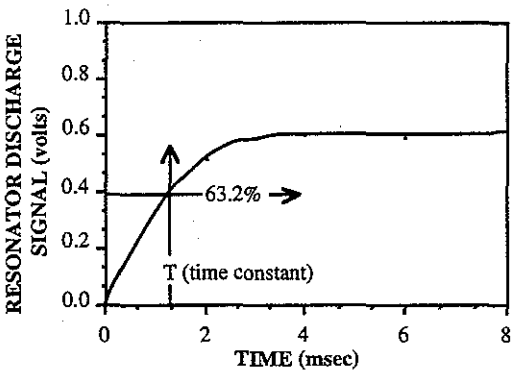

Fig. 8(b) Response curve of the discharge current subjected to a step input of 1 kW

Power Manipulation via the Model-based Optimization Strategy

Fig. 9(a) shows the power profile determined by the model-based optimization strategy for temperature stabilization when approaching a boundary. Fig. 9(b) and (c) show photographs taken of the kerf produced with and without the power control implementation. It is clear from the photographs that the quality of the cut at the beam exit is greatly improved by the control scheme.

Fig. 10(a) shows a typical power profile determined by the scheme for cornering. Fig. 10(b) and (c) show typical results when the optimization strategy was physically implemented. It is clear that corner melt-off is significantly reduced by adapting laser power in a non-linear fashion as determined by the optimization module.

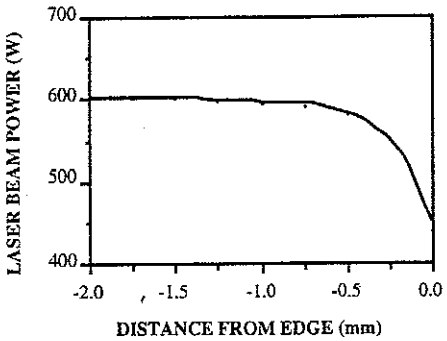

(a) Power profile required for temperature stabilization on boundary encroachment

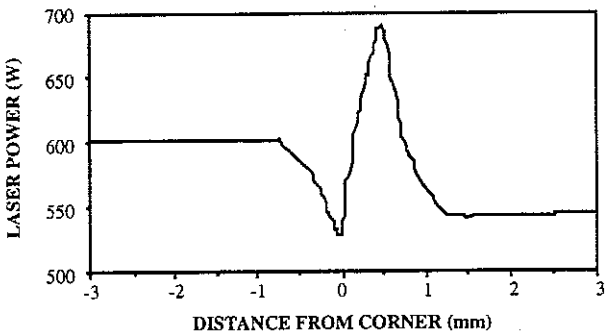

(a) Power profiles required for temperature stabilization when cornering

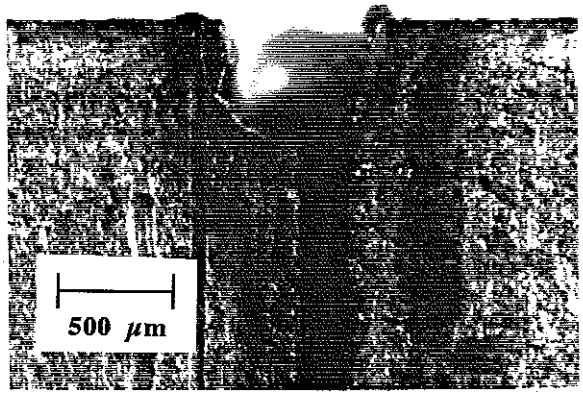

(b) Without power adaptation

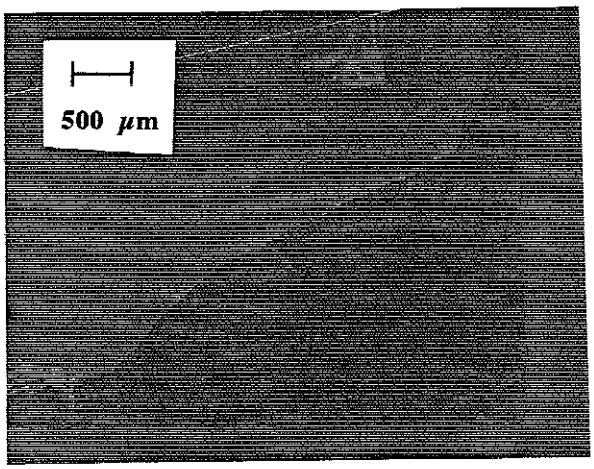

(b) Without power adaptation

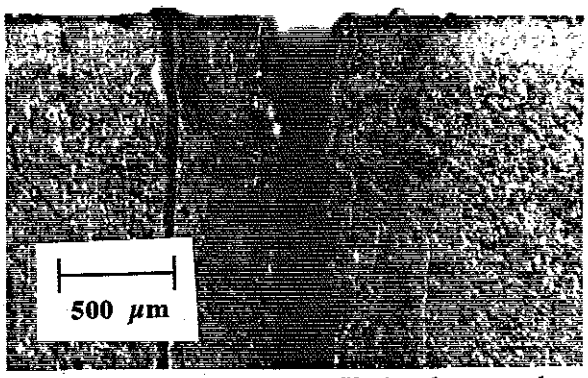

(c) With the power profile implemented

Fig. 9 Boundary encroachment (20mm/s)

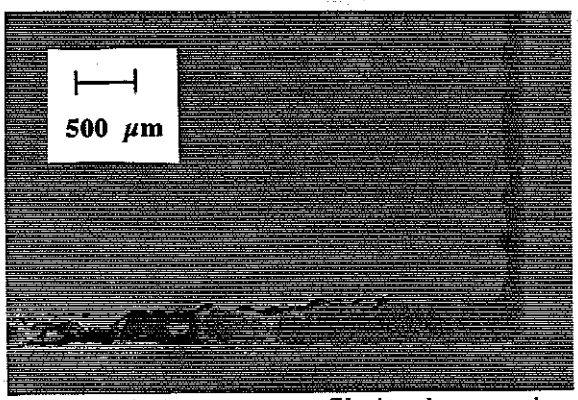

(c). With the power profile implemented

Fig. 10 Cornering (20mm/s)

Fig. 11(a) shows a typical power profiles determined for quality improvements in laser hole cutting. Such schemes are required to stabilize temperatures from initiation to termination as the process does not reach any steady-state equilibrium due to the progressive directional changes imposed and the kerf-limited diffusion associated with this condition. When this power profile was experimentally applied, no significant improvements in the geometry of the holes were detectable, but improvements were found in the extent of heat-affected zones surrounding the cut edges.

Evaluation of Heat-Affected Zones

Metallographic observation of the HAZ can be used to measure their extents. When analyzing laser-cut specimens, a common method of evaluating the HAZ is by measuring the visible surface oxidation mark (Steen and Kamalu, 1983, and Rajendran and Pate, 1988). Metallurgical HAZ's require considerably more effort to obtain in contrast. Nevertheless, the visible surface oxidation mark is a reliable indicator of thermo-physical change.

The prediction of HAZ's have been attempted by many (e.g., Glass et al., 1989, and Li and Sheng, 1995). In the work presented, the HAZ extent is defined as the visible surface oxidation mark, and therefore its prediction should be based on the temperature at which the surface undergoes chemical oxidation by the presence of the impinging gas stream. It was reported by Geiger et al. (1988) that the ignition point for such a reaction to occur in mild steel is 1473.15 K. Fig. 11(b) shows that by applying power adaptation profiles, actual HAZ's are reduced considerably over what is conventionally possible when power levels are maintained uniformly. It is also shown that there is good agreement between the predicted and actual HAZ's when the transitional temperature is taken as the ignition point of steel with oxygen.

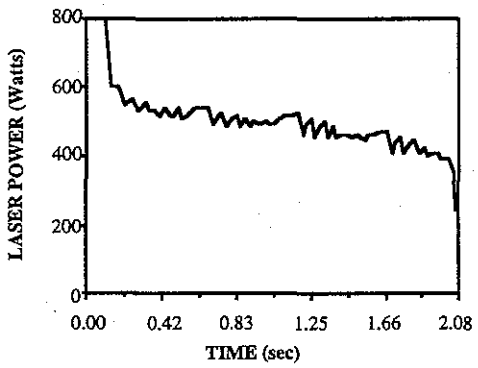

Fig. 11(a) Laser beam power profiles required for temperature stabilization when circular hole cutting (initial laser power: 800 W, cutting speed: 10mm/s)

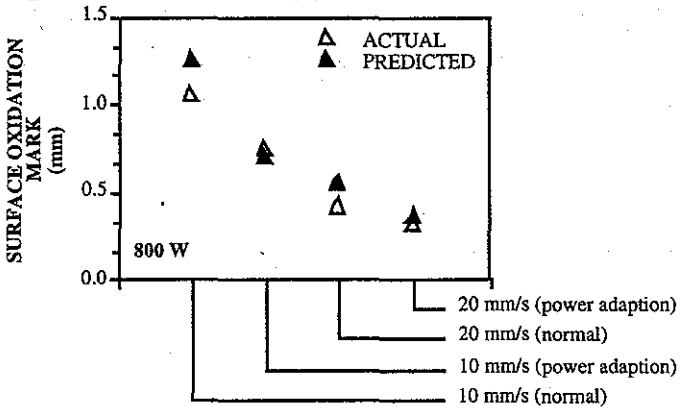

Fig. 11(b) Comparisons of actual heat-affected zones (with and without power adaptation) and numerically determined value

CONCLUDING REMARKS

The numerical model developed examined issues including cutting front mobility and temporal beam coupling effects. Bulk heating effects (due to cut geometry change including boundary encroachment, cornering and cutting small holes) caused the front velocity to vary, and beam coupling was significantly affected as a result. A model-based optimization strategy for improving laser cutting quality under these non-steady state conditions was presented. It endeavors to manipulate laser beam power in order to stabilize the cutting front temperature at these regions and thus eliminate the need for trial-and-error based experimentation which is currently adopted. Experimental results obtained from the control scheme show agreement with numerical prediction and also show significant improvement in quality through reduced kerf widening effects in boundary encroachment, reduced corner melt-off in cornering, and reduced HAZ extents when cutting small holes.

REFERENCES

Arata, Y., et al., (1979), "Dynamic behaviour in laser gas cutting of mild steel", *Trans. JWRI* **8** (2), 15-26.

Di Pietro, P., and Yao, Y.L., (1994), "An investigation into characterizing and optimizing laser cutting quality - a review", *Int. J. Mach. Tools Manufact.* **34** (2), 225-243.

Di Pietro, P., and Yao, Y.L., (1995), "A numerical investigation into cutting front mobility in CO_2 laser cutting", *Int. J. Mach. Tools Manufact.*, **35** (5), 673-688.

Geiger, M., et al., (1988), "Laser cutting of steel sheets", *Laser Assisted Processing*, SPIE **1022**, 20-33.

Glass, J.M., et al., (1989), "Heat transfer in metallic glasses during laser cutting", *Heat Transfer in Manufacturing and Materials Processing*, Trans. ASME, **HTD-113**, 31-38.

Gonsalves J.N., and Duley, W.W., (1972), "Cutting thin metal sheets with the CW CO_2 laser", *J. Appl. Phys.* **43** (11), 4684-4687.

Li, K., and Sheng, P., (1995), "Computational model for laser cutting of thin steel plates", *Proc. of ASME IMECE (WAM)*, San Francisco, USA, 12-17 Nov., MED-Vol. 2-1, 3-14.

Miyamoto, I., et al., (1984), "Intensity profile measurements of focused CO_2 laser beam using PMMA", *Proc. of ICALEO*, LIA **44**, 313-320.

Miyamoto, I., et al., (1986), "Beam absorption mechanism in laser welding", *Laser Processing: Fundamentals, Applications, and Systems Engineering*, SPIE **668**, 11-18.

Moriyasu, M., et al., (1986), "Adaptive control for high-speed and high-quality laser cutting", *Proc. of ICALEO*, 129-136.

Moriyasu, M., Hiramoro, S., Hoshinouchi, s., and Ohmine, M., (1986), Adaptive control for high-speed and high-quality laser cutting, *Proc. ICALEO'85*, 129-136.

Powell, J., (1993), *CO_2 Laser Cutting*. Springer, London, pp. 218-222.

Powell, J., *et al.*, (1992), The Role of Oxygen Purity in Laser Cutting of Mild Steel, *ICALEO*, Florida, USA, 1-10.

Rajendran, N., and Pate, M.B., (1988), "Real-time laser materials processing control: a feasibility study", *Laser Materials Processing*, Proc. of ICALEO, California, USA, 119-129.

Schreiner-Mohr, U., Dausinger, F., and Hugel, H., (1991), "New aspects of cutting with CO_2 lasers", *Proc. of ICALEO*, SPIE **1722**, 263-272.

Schuocker, D., (1988), Heat Conduction and Mass Transfer in Laser Cutting, *Laser Technologies in Industry*, SPIE Vol. 952, 592-599.

Schuocker, D., and Steen, W., (1986), "Advanced concepts in laser material processing in Europe", *Manufacturing Applications of Lasers*, SPIE **621**, 17-22.

Sheng, P., and Cai, L., (1994), "Model-based path planning for laser cutting of curved trajectories", *Int. J. Machine Tools and Manufacture*, Vol.36, No.6, 739-754.

Steen, W.M., and Kamalu, J.N., (1983), *Laser Materials Processing*, edited by M. Bass. North-Holland Publishing Co., The Netherlands, pp. 15-111.

Steen, W.M., and Li, L., (1988), "Some viewpoints on laser automation and processing quality control", *Laser Technologies in Industry*, SPIE **952**, 544-551.

White, F.M., (1988), Heat and Mass Transfer, Addison-Wesley, USA, 332-336.

Yuan, S.F., et al., (1988), "Thermical modelisation of laser cutting process", *Laser Technologies in Industry*, SPIE **952**, 583-591.

MEET THE AUTHORS

Dr. Paul Di Pietro received his PhD from the School of Mechanical and Manufacturing Engineering at University of New South Wales, Sydney, NSW, Australia in 1995. He is currently with Di Pietro & Sons Engineering, Fairy Meadow, NSW, Australia.

Dr. Y. Lawrence Yao has been an Associate Professor with the Department of Mechanical Engineering at Columbia University since 1994. Prior to joining Columbia, he was a Senior Lecturer at University of New South Wales. He received his MS and PhD from University of Wisconsin-Madison in 1984 and 1988, respectively.

Power Manipulation via the Model-based Optimization Strategy

Fig. 9(a) shows the power profile determined by the model-based optimization strategy for temperature stabilization when approaching a boundary. Fig. 9(b) and (c) show photographs taken of the kerf produced with and without the power control implementation. It is clear from the photographs that the quality of the cut at the beam exit is greatly improved by the control scheme.

Fig. 10(a) shows a typical power profile determined by the scheme for cornering. Fig. 10(b) and (c) show typical results when the optimization strategy was physically implemented. It is clear that corner melt-off is significantly reduced by adapting laser power in a non-linear fashion as determined by the optimization module.

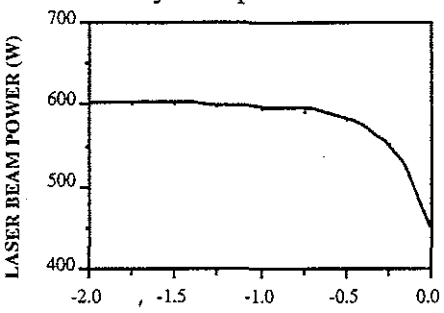

(a) Power profile required for temperature stabilization on boundary encroachment

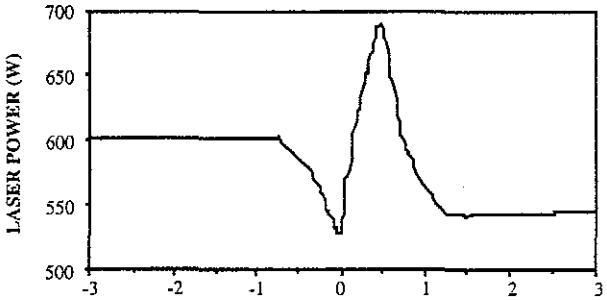

(a) Power profiles required for temperature stabilization when cornering

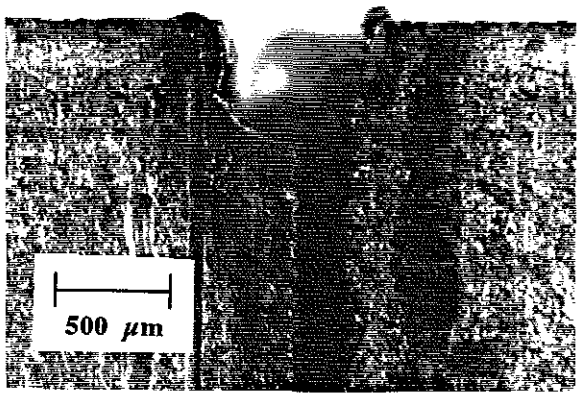

(b) Without power adaptation

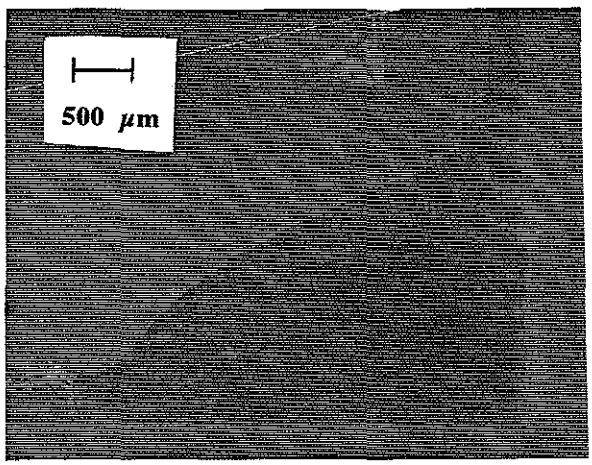

(b) Without power adaptation

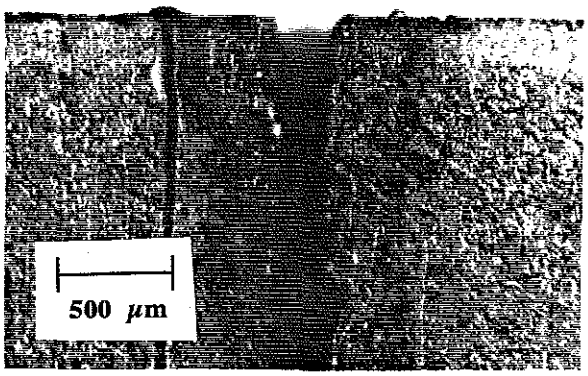

(c) With the power profile implemented

Fig. 9 Boundary encroachment (20mm/s)

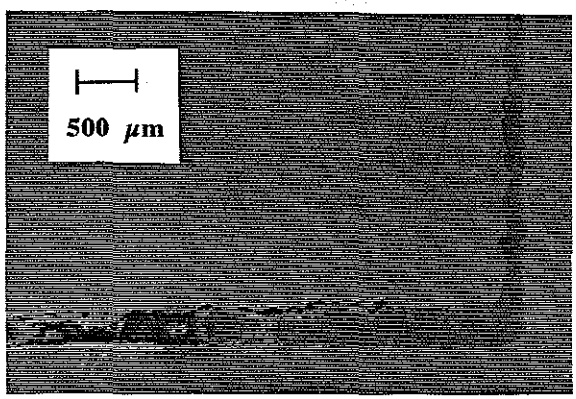

(c). With the power profile implemented

Fig. 10 Cornering (20mm/s)